

УДК 534.2, 622.02

## ON THE ORIGIN OF SEISMIC ANISOTROPY IN ROCKS. EXPERIMENTAL AND THEORETICAL STUDIES ON BIOTITE GNEISS SAMPLES

I.Yu. Zel<sup>1,2</sup>, T.I. Ivankina<sup>1</sup>, T. Lokajicek<sup>3</sup>, H. Kern<sup>4</sup>, D.M. Levin<sup>2</sup>

<sup>1</sup>Frank Laboratory of Neutron Physics, Joint Institute for Nuclear Research, Dubna, Russia

<sup>2</sup>Tula State University, Tula, Russia

<sup>3</sup>Institute of Geology Academy of Sciences Czech Republic, Prague, Czech Republic

<sup>4</sup>Institute of Earth Sciences, University of Kiel, Germany

**Abstract.** The paper presents the results of experimental and theoretical investigations on highly anisotropic sample of plagioclase-biotite gneiss with structure of compositional layering and biotite gneiss sample of weak anisotropy. Two acoustic methods were used for measuring seismic anisotropy: measurements of P-wave ray velocities on a sphere and comprehensive measurements of P- and S-wave phase velocities on a cube under different confining pressures. The combination of P-wave velocity spatial distribution with S-wave velocities in three orthogonal directions was used to recover the elastic moduli of anisotropic rock samples.

The crystallographic textures of major rock-forming minerals were measured by the method of neutron diffraction. On the basis of texture data was performed the theoretical modeling of elastic properties using different averaging methods and theories of effective properties of microheterogeneous media.

In this work for the first time the authors implemented a nonlinear approximation of the P-wave velocity-pressure relation for estimation of mineral matrix properties and orientation distribution of microcracks. From the theoretical modeling it was found that the bulk elastic anisotropy of the sample is caused by the preferred orientations of micas grains and microcracks.

The comparison of theoretical calculations with ultrasonic measurements showed large discrepancies in S-wave velocities.

**Keywords:** biotite gneiss, elastic wave velocities, crystallographic texture, compositional layering, seismic anisotropy.

### Introduction

Seismic anisotropy shows itself in propagation of elastic waves of different polarization in anisotropic rocks both in seismic observations and in laboratory experiments [Aleksandrov, Prodajvoda, 2000; Ivankina, Matthies, 2015; Babuska, Cara, 1991]. In laboratory conditions the study of seismic anisotropy is carried out using ultrasonic sounding by means of elastic waves registration propagating through the rock sample in different directions. However, to identify factors affecting the anisotropy of elastic properties, the comprehensive approach is necessary including additional experimental and theoretical research methods.

Rock is a heterogeneous polycrystalline medium which elastic anisotropy depends on microstructure characteristics including preferred orientation of mineral grains (crystallographic texture), their shape (shape texture), composition layering, system of oriented microcracks and grain boundaries.

Measuring of crystallographic texture of rock using neutron diffraction allows us to carry out a full quantitative texture analysis, i.e. to determine the preferred orientation of existing grains of main rockforming minerals [Ivankina, Matthies, 2015].

Sharpness of texture and elastic anisotropy of minerals themselves are the main reasons of seismic anisotropy observed at high confining pressures in lithosphere rocks [Babuska, Cara, 1991]. It is important that at low pressures (close to atmospheric), elastic waves are

sensitive to the presence of nonspherical pores and microcracks. Therefore, the total elastic anisotropy will additionally depend on orientation shape and volume content of microcracks [Ivankina and Matthies, 2015; Kern et al., 2008; Vasin et al., 2013].

The shape of grains as well as shape of fractures also should be regarded as a source of seismic anisotropy. For tabular minerals, such as for example, biotite and muscovite, the shape texture is associated with crystallographic texture. In this regard, in theoretical simulation the influence of grain shape can be considered on the basis of data about crystallographic texture [Ivankina and Matthies, 2015; Vasin et al., 2013].

Compositional layering which is an alternation of layers with different properties, on the one hand, refers to the texture shape, because layers are ordered objects of defined form. On the other hand, layering is an example of natural spatial inhomogeneity that distinguishes it from other factors. The only experimental confirmation of layering influence on elastic anisotropy obtained on artificial samples consisting of layers of epoxy resin and glass, is given by Melia and Carlson [1984]. Despite the fact that the study of anisotropy of rocks elastic properties are the subject of many works, the factor of compositional layering remains so far poorly understood. Moreover, the approaches themselves to identify the causes of seismic anisotropy in complex structured rocks under different confining pressure [Bayuk and Ryzhkov, 2010; Kern et al., 2008; Vasin et al., 2013] are limited either by the number and completeness of experimental data, or by methods of theoretical simulating.

Below are given the results of experimental and theoretical studies of gneisses with different structural properties. One of them (sample *PL3670*) is a highly anisotropic plagioclase-biotite gneiss with compositional layered structure; the other one (sample *OKU2*) is a homogeneous biotite gneiss with defined foliation.

### **Description of samples**

Experimental studies were carried out on samples of spherical (Fig. 1, *a*) and cubic (Fig. 1, *b*) form. The diameter of spherical sample is 50 mm, the height of cube face is 43 mm. Coordinate system XYZ for the studied samples was chosen according to structural (at descriptive level) characteristics of rocks: Z axis is perpendicular to foliation plane; X and Y axes lie in the foliation plane and are oriented parallel (X axis) and perpendicular (Y axis) to lineation (position of coordinate axes see at Fig.1, *b*).

The sample of biotite gneiss *OKU2* selected from the investigation well in Outokumpu (Finland) from a depth of 409 m [Kern et al., 2009] contains 39.6% of quartz, 36.9% of plagioclase, and 23.4% of biotite. The microstructure of the sample is represented by impregnations of biotite grains in quartz-plagioclase matrix (Fig. 1, *d*).

The sample of plagioclase-biotite gneiss *PL367* selected from the surface on the section of Musta Tunturi (Kola Peninsula) is analogous to Archean rocks from the Kola superdeep borehole [Lobanov et al., 2002]. Sample contains 30.6% of quartz, 28.8% of oligoclase, 20.9% of biotite, 16.3% of muscovite, and 3.4% of sillimanite. Unlike sample *OKU2* in this sample grains of biotite and muscovite form nearly parallel layers, which can be traced throughout the volume of the sample (Fig. 1, *c*) according to the data of neutron radiography carried out at Frank Laboratory of Neutron Physics in Dubna [Kichanov et al., 2015],

### **Experimental methods**

*Measurement of velocities of elastic waves.* Two experimental approaches were used to measure velocities of elastic waves. First, in the Geological Institute of the Academy of Sciences of Czech Republic, the measuring of *P*-wave velocities was performed on spherical

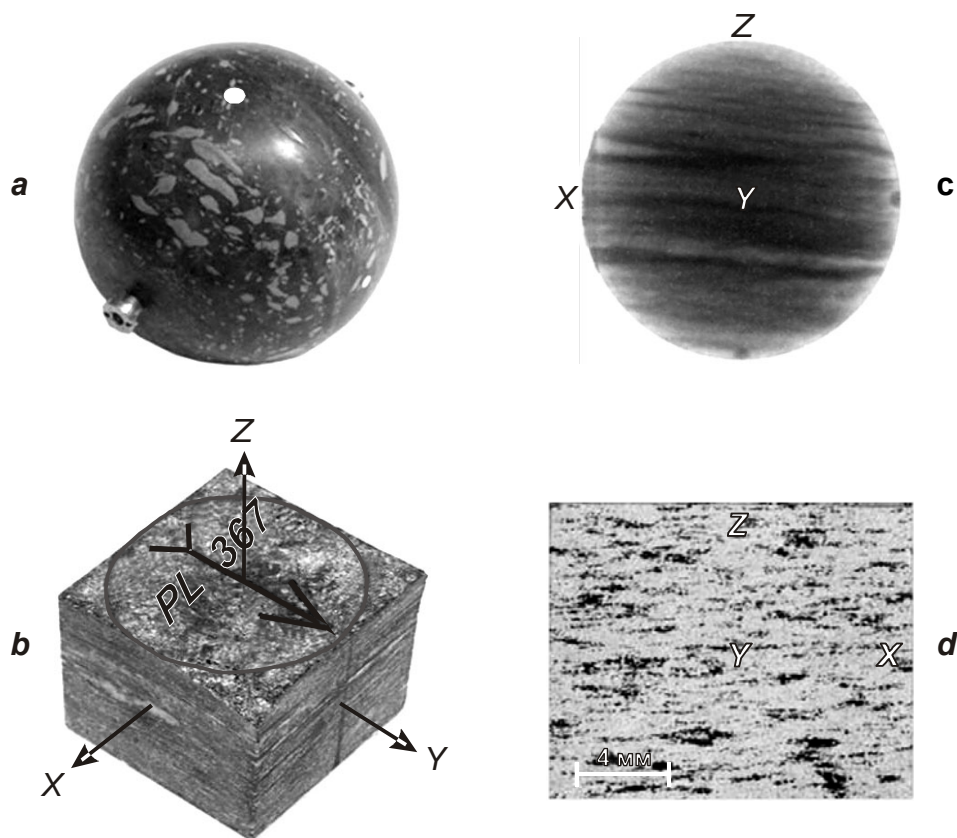


**Fig. 1.** (a) Spherical sample; (b) cubic sample with XYZ axes; (c) neutron-radiographic image of layered gneiss *PL367*; and (d) micropicture of thin section of ZX plane of foliate gneiss *OKU2*. Dark color in *b*, *d* corresponds to the most absorbing minerals (micas).

samples with diameter of 50 mm in 150 directions at confining quasi-hydrostatic pressure up to 400 MPa [Lokajicek, Svitek, 2015]. Measurements were performed with a pair of ultrasonic ( $F=2$  MHz) transducers (source-receiver) disposed diametrically on spherical surface of the sample. The directions of measurements were set by angles  $\lambda$  and  $\varphi$ . The first one determines displacement of a pair of transducers around horizontal axis with a step of  $15^\circ$  in the interval of  $\lambda$  values from 0 to  $75^\circ$  (Fig. 2, *a*). Angle  $\varphi$  describes rotation of the sample around vertical axis at  $360^\circ$  with the same step (Fig. 2, *b*). Due to the rotation of a sample for each fixed position of the source-receiver, directions of measurements of elastic waves form a cone (Fig. 2, *a*). The number of independent directions of measurements is 132. All measuring construction is placed inside the chamber of high pressure that is filled with oil to create a quasi-hydrostatic pressure on the sample.

The second approach carried out in the Institute of Earth Sciences, University of Kiel (Germany), involves the measuring of *P*- and *S*-wave velocities on cubic samples in three directions under triaxial compression up to 400 MPa. The pressure was created by hydraulic frames and was transmitted to the samples through anvils in three mutually perpendicular directions ( $\sigma_1, \sigma_2, \sigma_3$ ). The system of three transducers (*P*-sensor with frequency of 2 MHz and two *S*-sensors with frequency of 1 MHz) for measuring velocities of *P*- and *S*-waves propagating in one direction was located at each face of the cubic sample from the side of anvils. As a result, three phase velocities  $V_P$  and six phase velocities  $V_S$  were measured in directions perpendicular to sample faces (Fig. 3). In more details the principle of measuring and description of installation are represented in [Kern, 1982].

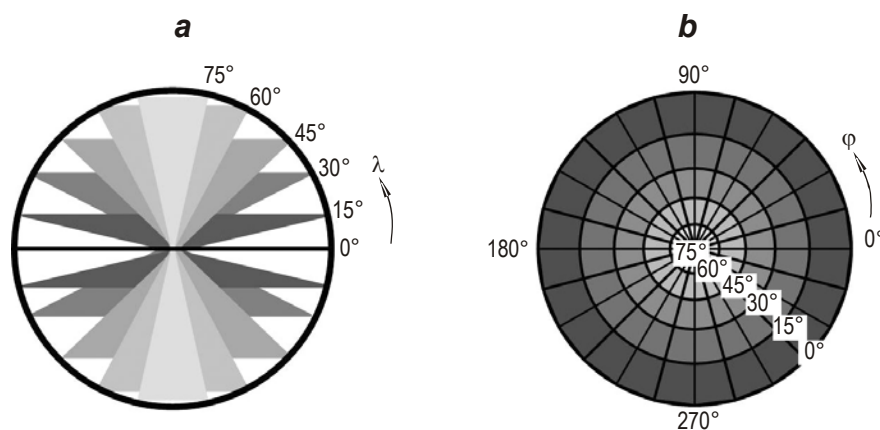


**Fig. 2.** (a) Cones of directions and (b) stereographic projection corresponding to  $P$ -wave measuring on spherical sample.  $\lambda$  is an angle determining the displacement of pair of transducers around the horizontal axis with the step of  $15^\circ$  in the interval of  $\lambda$  values from 0 to  $75^\circ$ ;  $\varphi$  is an angle describing the rotation of the sample with the same step around the vertical axis at  $360^\circ$

*Determination of elastic moduli using values of elastic waves velocities.* Results of ultrasonic measurements on the samples usually confirm the existence of seismic anisotropy in rocks. However, a quantitative description of elastic anisotropy of the sample assumes determination of regularity between experimental values of elastic wave velocities and the tensor of elastic moduli. Determination (recovery) of elasticity tensor components by limited set of measured velocity values allows to calculate the velocities of differently polarized waves and also any other elastic characteristics of anisotropic medium.

In our case, velocity values measured on spherical and cubic samples were used to calculate elastic moduli. It has been already noted that the ray  $P$ -wave velocities were obtained in 132 independent directions and phase  $S$ -wave velocities, in three directions, which is sufficient to determine all the 21 components of elasticity tensor [Zel et al., 2015, 2016].

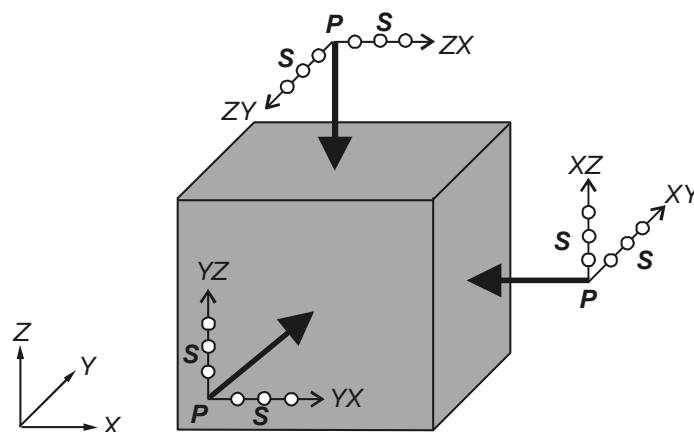


**Fig. 3.** Scheme of ultrasonic measurements of  $P$ - and  $S$ -wave velocities on the cubic sample using transducers of different polarization

$XYZ$  is a coordinate system. Solid black arrows are directions of propagation of  $P$ -waves; arrows with white circles are directions of propagation of  $S$ -waves and their polarization (for example, for two  $S$ -waves ( $XZ$  and  $XY$ ) propagating in direction  $X$ , polarization will occur in directions  $Z$  and  $Y$ )

The elastic moduli were calculated in two stages. First,  $P$ -waves velocities measured in 132 directions on spherical sample were used to calculate 9 independent components of elasticity tensor and 6 different combinations of elastic moduli. Then, based on already obtained values of elastic moduli, missing 12 independent tensor components were determined using 6 velocity values of  $S$ -waves measured on the cubic sample.

*Neutron-diffraction measurements of crystallographic textures.* Preferred orientation of grains in main rockforming minerals of two samples of biotite gneisses was measured by neutron diffraction method at the texture diffractometer SKAT (reactor IBR-2) in the Institute of Nuclear Research, Dubna, Russia [Keppeler et al., 2014]. The detector ring with the dispersion angle  $2\theta=90^\circ$  was used for the samples studied. The registration of diffraction peaks was performed simultaneously for all 19 detectors; exposure time was 60 min. The sample was rotated with the step of  $10^\circ$ , which provided 684 diffraction spectra. Further these diffraction data, spectra of diffraction dispersion of neutrons, were used to construct the experimental pole figures (PF).

## Results of the experiments

*Determination of velocity anisotropy of longitudinal and transverse waves.* Some results obtained for the samples *OKU2* and *PL367* on the basis of ultrasonic measurements and the elasticity tensor determination are presented in Fig.4.

To determine the anisotropy of velocities of the longitudinal waves  $V_P$  the coefficient  $A$  was used [Birch, 1961]:

$$A = \frac{V_{\max} - V_{\min}}{V_{\text{mean}}} \cdot 100\% ,$$

where  $V_{\max}$ ,  $V_{\min}$ , and  $V_{\text{mean}}$  are the maximum, minimum, and average velocity values. For shear waves the main indicator of the anisotropy degree is splitting  $dV_S = V_{S1} - V_{S2}$  [Crampin, 1981] observed in the directions, along which two shear waves propagate with velocities  $V_{S1}$  (fast  $S$ -wave) and  $V_{S2}$  (slow  $S$ -wave).

According to the contour maps of  $P$ - and  $S$ -wave velocities, the sample *OKU2* is characterized by the orthorhombic symmetry of elastic properties (Fig. 4, *a*) and the sample *PL367*, by the nearly transversely isotropic symmetry (Fig. 4, *b*). For both samples, the plots, given in Fig.4, *c*, show the nonlinear increase in  $P$ -wave velocities with the pressure increase. The greatest differences between the properties of the samples are observed in behavior of elastic  $P$ -waves propagated perpendicular to  $XY$  plane (plane of foliation and layering) with minimum velocities  $V_{P\min}$ , which also influences the coefficient  $A$ . For the sample *OKU2*, the coefficient  $A$  is 13 % at 0.1 MPa and slightly decreases, approximately, by 2 % with the pressure increase (Fig. 4, *c*, *left*). Significant changes in velocities  $V_{P\min}$  in the sample *PL367* ( $\sim 2$  km/s) observed at pressure increase up to 50 MPa lead to the decrease in anisotropy coefficient from 51 % to 19 % (Fig. 4, *c*, *right*).

Special attention should be paid to considerable differences in values of  $V_S$  depending on directions of propagation of  $S$ -waves in the samples. Maximum values of  $V_{S1}$  and  $dV_S$  are observed in directions that differ from  $X$  and  $Y$  directions of the structure system of coordinates. In  $Z$  direction, perpendicular to the foliation plane and layering,  $V_{S1}$  and  $dV_S$  become minimal in both samples. In general, the calculated distributions of  $V_{S1}$  and  $dV_S$  for two samples are characterized by similar contours that slightly change with the pressure increase.

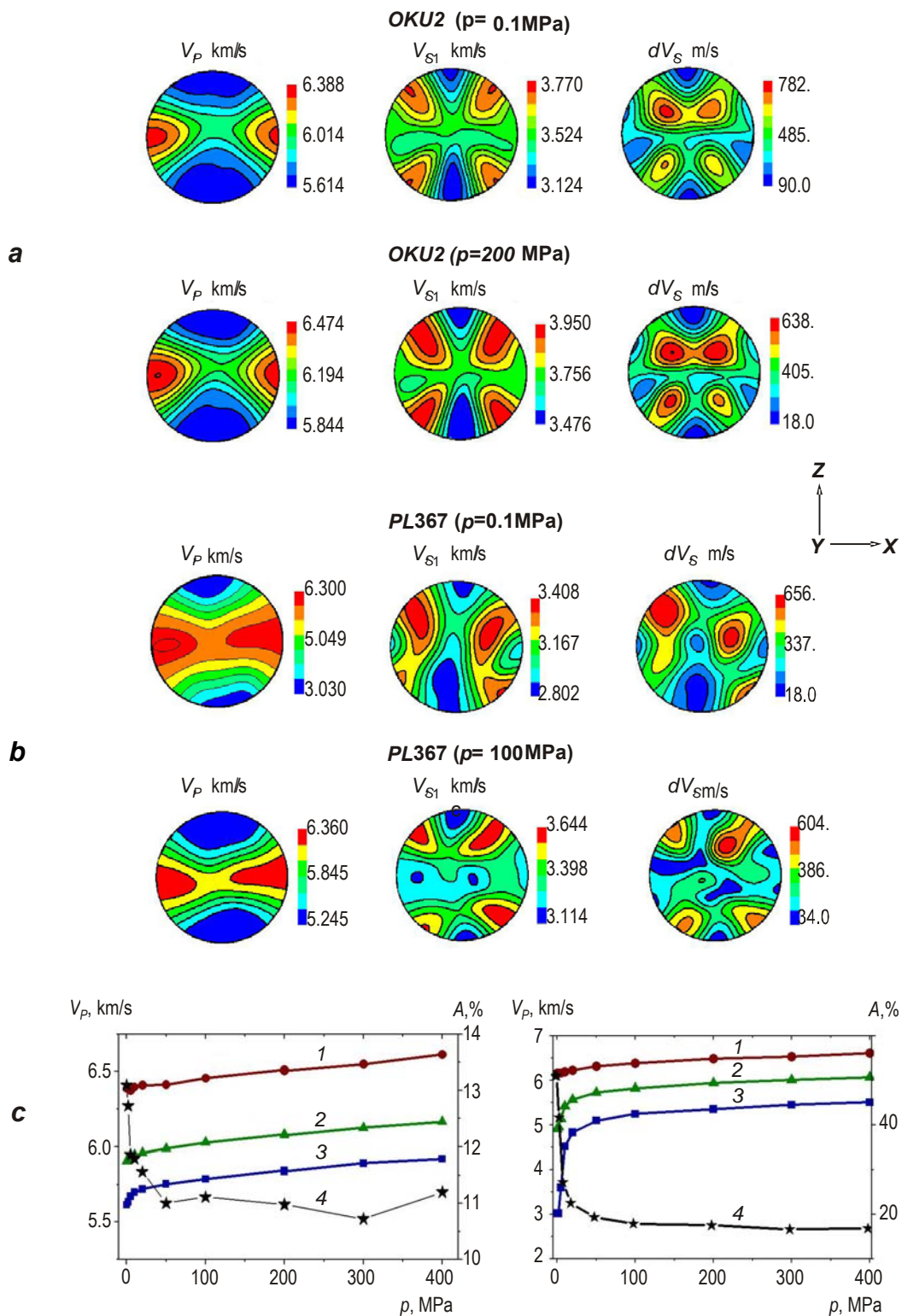


**Fig. 4.** Contour maps (stereographic projection) of phase velocities  $V_P$  and  $V_{S1}$  and splitting  $dV_S$  of  $S$ -wave velocities calculated from the components of elasticity tensor restored: (a) sample *OKU2* at pressure  $p=0.1$  MPa (atmospheric) and  $p=200$  MPa and (b) sample *PL367* at pressure  $p=0.1$  MPa (atmospheric) and  $p=100$  MPa; c is dependences of the maximum (line 1), average (line 2), minimum (line 3) velocity values  $V_P$ , and coefficient of anisotropy  $A$  (line 4) on pressure for the samples *OKU2* (left) and *PL367* (right)

*Nonlinear approximation of dependence of elastic waves velocity on pressure.* The presence of pores and microcracks in the rocks significantly influences the anisotropy of elastic properties, resulting, for example, in nonlinear changes in elastic properties of the sample under the uniform pressure (Fig. 4, *c*). The compression of the porous sample leads to the decrease of volume of pores and microcracks. The observed dependence of elastic properties on pressure can be used to determine the elastic properties of mineral matrix and orientation of microcrack system, for example, with nonlinear approximation of dependence of *P*-wave velocities on pressure:

$$V_p = V_{p0} + Bp - D \exp(-k \cdot p), \quad (1)$$

where *p* is uniform pressure;  $V_{p0}$  and  $B = \frac{\partial V_p}{\partial p}$  are the velocity and its change under pressure

corresponding to the elastic properties of mineral matrix at zero (atmospheric) pressure ( $p=0$ ,  $D=0$ ); *D* and *k* are the parameters describing the influence of cracks and pores ( $p=0$ ).

This approximation was applied to the phase velocities of *P*-waves calculated after determination of elastic moduli of samples in 132 directions. Figure 5 shows the obtained spatial distributions of parameters  $V_{p0}$ , *B*, *D*,  $1/k$  for the samples *OKU2* and *PL367*. Contour maps of  $V_{p0}$  for both samples show the symmetry and anisotropy similar to the experimental distributions of *P*-wave velocities at high pressures (see Fig. 4). Thus, there is reason to consider that elastic properties of mineral matrix can be described by experimental velocity values obtained at  $p=200$  MPa on the sample *OKU2* and  $p=100$  MPa on the sample *PL367*.

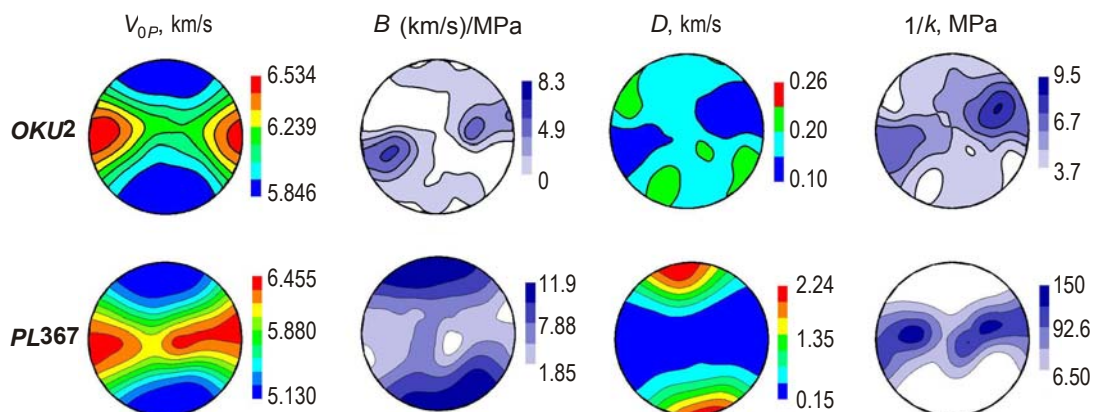


**Fig. 5.** Three-dimensional distributions (stereographic projection) of parameters of nonlinear approximation for the samples *OKU2* (*top*) and *PL367* (*bottom*); first column is  $V_{p0}$ ; second, *B*; third, *D*; and fourth,  $1/k$ . Coordinate system *ZXY* is similar to the system in Fig. 4

It can be seen that the distribution of parameter *D* for the sample *PL367* has a characteristic maximum concentrated near *Z* axis with a deviation from it of about  $15^\circ$  (Fig. 5, *bottom* row). Apparently, at  $p=0.1$  MPa, orientation of microcracks in this sample has a preferred direction that affects the nature of *D* distribution.

In contrast to the sample *PL367*, the range of velocity changes of *P*-waves in the sample *OKU2* is not significant (the maximum of *D* parameter is about 270 m/s). However, for this sample the distribution of *D* itself is not uniform and has defined poles of minimum values (Fig. 5, *top* row), that also indicates the possible preferred orientation of microcrack system or elongated pores.

The results of measurements of crystallographic texture. Texture measurements of biotite gneiss and plagioclase-biotite gneiss were performed on spherical samples. On the basis of neutron-diffraction data using the *WIMV* algorithm [Ivankin and Matthies, 2015], distribution functions of grains orientations (DFO) were calculated for all rock-forming minerals. Then using DFO in biotite and muscovite for the main crystallographic planes (001), (010), and (100), the pole figures (PF) were calculated, reflecting the well-developed sharp texture (Fig. 6).

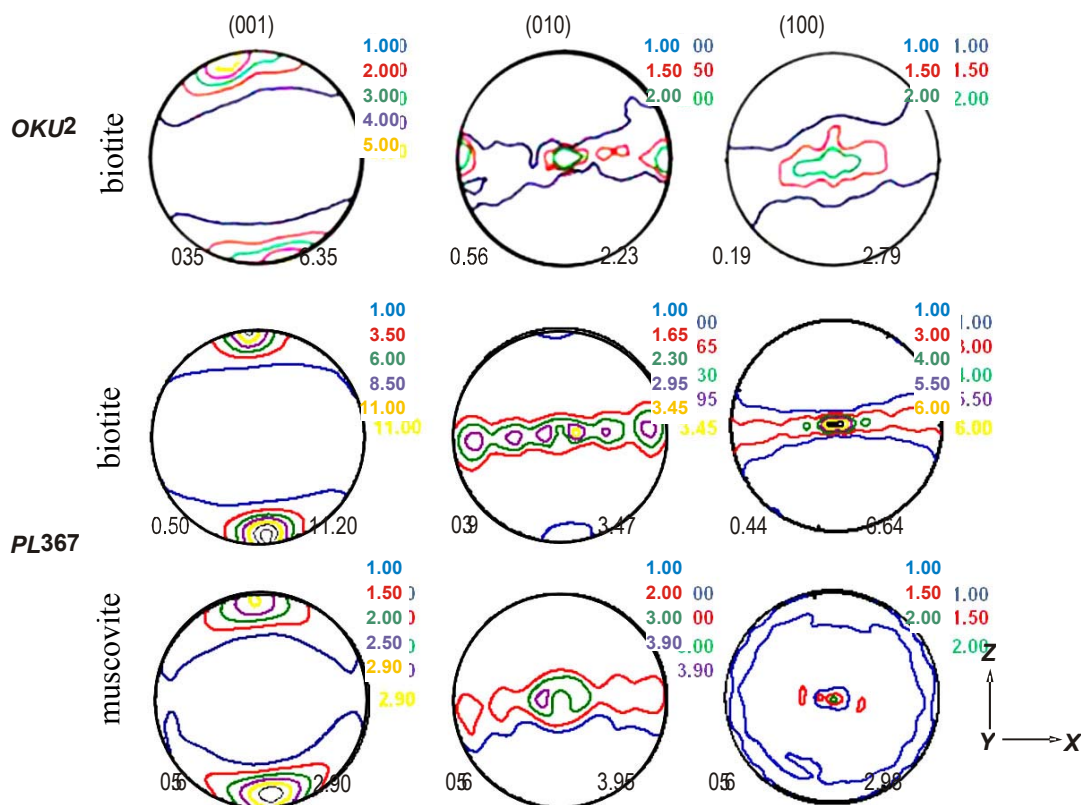


**Fig. 6.** The pole figures (PF) of basic crystallographic planes obtained from neutron-diffraction data in the samples *OKU2* (first row) and *PL367* (second and third rows) for biotite and muscovite. Stereographic projections are presented. Numbers under PF are minimum (left) and maximum (right) values of the pole density expressed in m.r.d.

In both samples, the maximum of pole density of plane (001) distribution in mica grains is oriented almost perpendicular to foliation plane with angle of inclination to *Z* axis at 10–15°. The preferred orientation of planes (010) and (110) forms belts parallel to the foliation plane that leads to the formation of nearly axial texture. The most sharp texture has biotite in the sample *PL367* with maximum of pole density in PF (001) equal to 11.2 m.r.d.<sup>1</sup> that is almost two times higher than the similar maximum in the sample *OKU2* amounting to 6.35 m.r.d.

Crystallographic textures of quartz and plagioclase in both samples are weak and are characterized by asymmetric distribution of pole density relative to the structural coordinate system *XYZ*.

<sup>1</sup> m.r.d. – units, that are multiples of random distribution

## Theoretical modeling of elastic anisotropy

*Mathematical models of elastic anisotropy of mineral matrix.* Simulating of elastic properties of micro-inhomogeneous medium, for example, of rocks, is based on calculating effective properties of some homogeneous medium [Shermergor, 1977]. The simplest models are evaluations of Voigt and Reuss assuming the homogeneity of strains or stresses at every point of the medium. Such approaches provide the upper and lower estimates of values of elastic properties. In order the resulting values will satisfy these estimates, the arithmetic and geometric average of elastic tensors in the approximations of Voigt and Reuss were proposed to be used.

More sophisticated methods (method of self-consistency, singular approximation, *GEO-MIX-SELF (GMS)* etc), based on Eshelby solution for ellipsoidal inclusion, allow to consider the shape of grains and their orientation [Ivankina and Matthies, 2015]. Solution of the problem of effective elastic properties of layered media was obtained by Backus [1962] for a model of isotropic layers and later on was generalized to the case of arbitrary anisotropic layers by Schoenberg and Muir [1989].

To estimate the impact of various factors on the elastic anisotropy of the samples *OKU2* and *PL367* modeling of elastic properties was performed using different approaches.

First the elastic properties of the models of mineral skeleton were calculated that do not contain pores and microcracks. Averaging taking into account only crystallographic texture of mineral grains (DFO) was carried out by the method of geometric average (model *GEOMEAN*). Elastic moduli of monocrystals of biotite, muscovite, quartz, sillimanite, and oligoclase (number An29 in the row of plagioclases) taken from the reference materials [Bass, 1995] were used for the calculations.

The influence of the shape of mica grains (muscovite and biotite) on the elastic properties of the sample were simulated by the *GEO-MIX-SELF (GMS)* method [Ivankina, Matthies, 2015; Vasin et al., 2013] that involves the self-consistency method and geometric averaging. The estimated model (*GMS* model) is a weakly anisotropic matrix that consists of plagioclase, quartz, and sillimanite<sup>1</sup> and includes impregnations of mica grains (muscovite and biotite) in the form of ellipsoidal inclusions. The elastic properties of the matrix were determined by the *GEOMEAN* method. The shape of the mica grains (muscovite and biotite) was described as an ellipsoid with parameters {1:1:0.05} for the sample *OKU2* and {1:1:0.01} for the sample *PL367*. It was also assumed that the distribution of the grain shapes by orientations coincides with crystallographic texture (DFO) of the grains themselves.

Model with compositional layering (*Backus* model) was calculated on the basis of general formulation for the anisotropic layers [Schoenberg, Muir, 1989]. The samples were regarded as a layered medium, where some layers were formed by textured grains of biotite and muscovite with elastic properties calculated by the *GEOMEAN* method, and the other are textured grains of plagioclase, quartz and sillimanite (the latter is in the case of sample *PL367*) with properties calculated by the same method.

The results of calculations of elastic properties of the samples are presented in Figs. 7 and 8.

It follows from the spatial distribution of  $V_P$  velocities (see the first columns in Figs. 7 and 8), that the volumetric elastic anisotropy of the samples is mainly controlled by crystallographic textures of biotite and muscovite. Effective elastic properties of different

---

<sup>1</sup> Sillimanite was presented in the form of randomly oriented crystallites in the sample *PL367*.

theoretical models of mineral matrix (*GEOMEAN*, *GMS*, *Backus*) differ insignificantly for both samples. The largest differences (about 6 %) between models are observed only for the spatial distributions of velocities of elastic  $S$ -waves  $V_{ST}$ : positions of maximums and velocity values in these directions differ noticeably. Comparison of results of theoretical modeling presented in Figs. 7 and 8 with experimental data (Fig. 4) indicates significant differences: about 10 % for  $P$ -wave velocities and almost 50 % for the splitting  $dV_S$

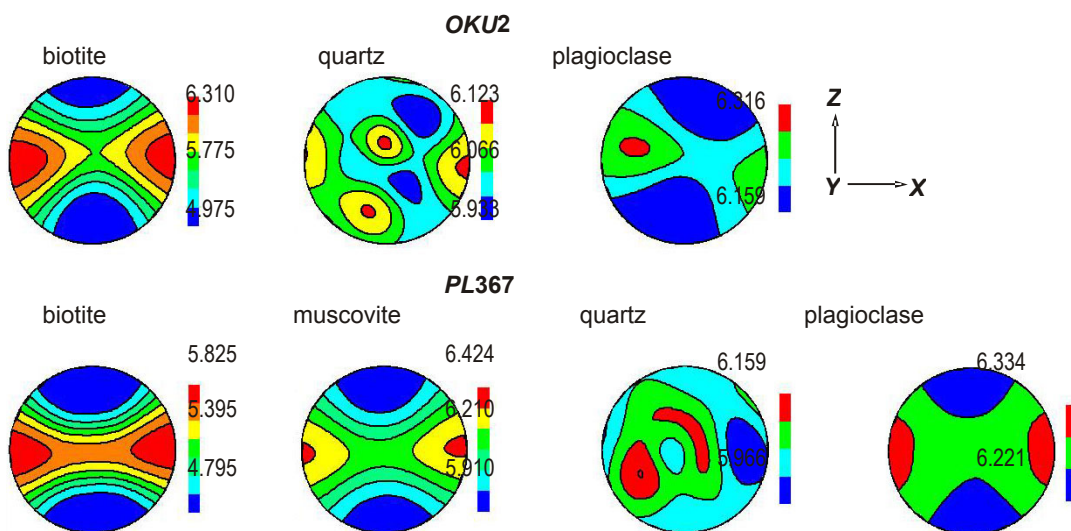


**Fig. 7.** Spatial distribution of phase velocities  $V_p$ , km/s (stereographic projection) for mineral components of two samples obtained using the *GEOMEAN* method.

*Mathematical models of elastic anisotropy with taking into account pores and cracks.* The next step was the modeling of effective properties of the samples taking into account the presence of pores and microcracks. The model of textured mineral matrix was proposed with inclusions of two types of pores – spherical and elongated in the form of ellipsoid (microcracks). The parameters of ellipsoid used for the sample OKU2 were  $\{1.1.0.1\}$  and, for the sample PL367,  $\{1.1.0.005\}$ .

The elastic moduli calculated using DFO (*GEOMEAN* for the sample OKU2 and *Backus* for PL367) were applied to describe the properties of mineral matrix of the samples (without pores and cracks). The further comparison involved elastic moduli of the samples calculated from the experimental data obtained at  $p=200$  MPa for the sample OKU2 and at  $p=100$  MPa for the sample PL367.

The influence of pores and microcracks on the elastic properties of the sample was simulated by the *GMS* method, where the elastic moduli of inclusions (voids) were supposed to be equal to zero. Estimation of microcracks part in the total porosity of the samples was performed as follows.

The density of the sample OKU2 measured at the atmospheric pressure is  $2.724 \text{ g/cm}^3$  that is close to the density value  $\rho_m$ , calculated from the mineral composition ( $2.742 \text{ g/cm}^3$ ). The sample PL367 contains more mica in comparison with the sample OKU2, that is why its density is higher and is equal to  $2.768 \text{ g/cm}^3$  at  $p=0.1$  MPa; the mineral density is  $\rho_m=2.809 \text{ g/cm}^3$ .

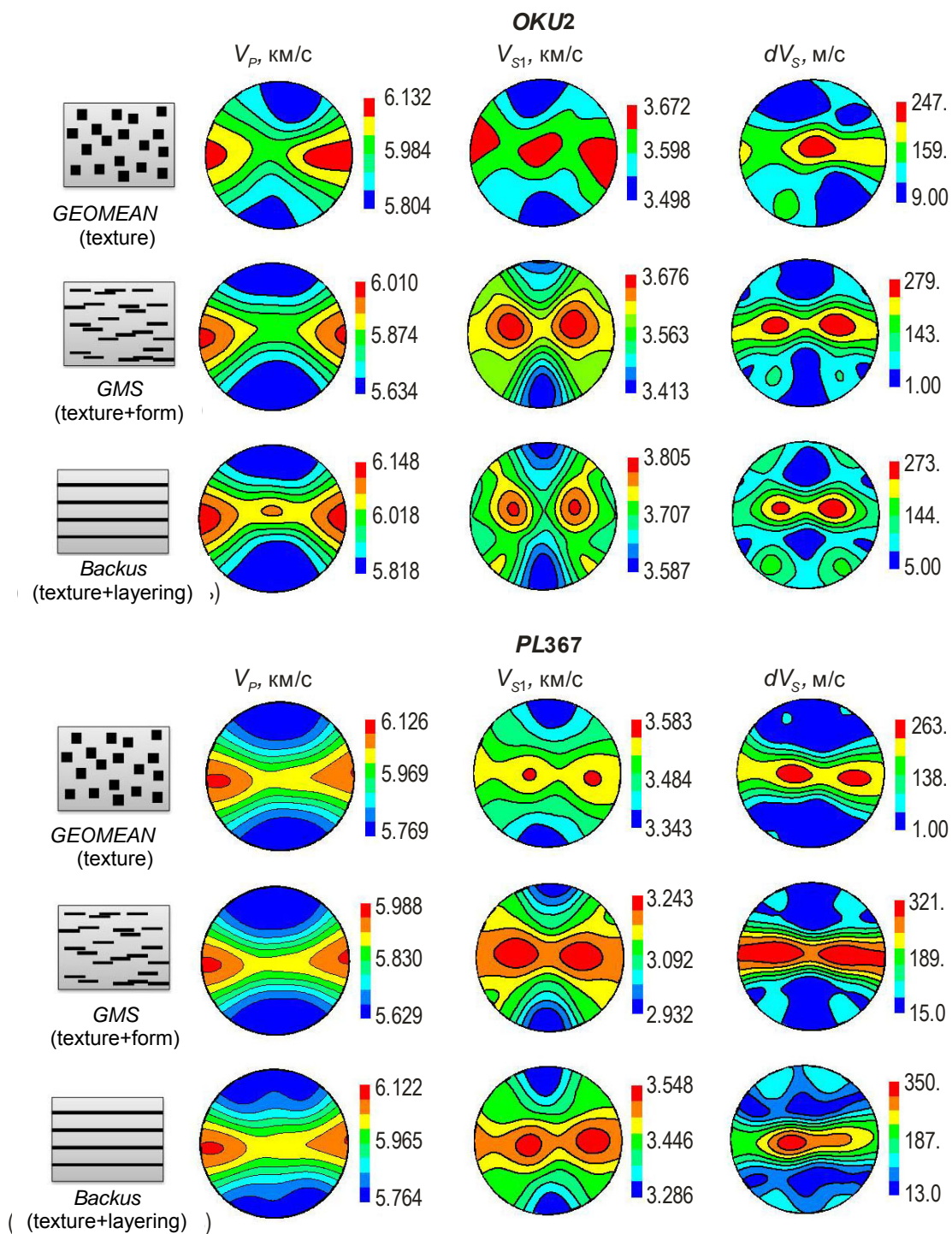


**Fig. 8.** Surfaces (stereographic projection) of phase velocities  $V_P$  (first column),  $V_{S1}$  (second), and splitting  $dV_S$  (third) calculated using the mathematical *GEOMEAN*, *GMS*, and *Backus* models for the samples *OKU2* (top) and *PL367* (bottom)

The porosity value calculated by the formula

$$\phi = \left( 1 - \frac{\rho}{\rho_m} \right) \cdot 100\% \quad (2)$$

at the atmospheric pressure is  $\sim 0.7\%$  for the sample *OKU2* and  $1.6\%$  for the sample *PL367*.

In case of the sample *PL367*, the smallest difference between experimentally measured *P*-wave velocities and distribution of  $V_{P0}$  corresponds to the experiment at the pressure of 100 MPa. Therefore, it was assumed that at 100 MPa, all microcracks (plane elongated pores) in the sample volume are closed and do not affect its elastic properties. Density measurement of *PL367* was performed simultaneously with measurement of velocities of elastic *P*- and *S*-waves throughout the range of uniform pressure on the cubic sample (see Fig. 3, *c*). At a pressure of 100 MPa, the density value is 2.783 g/cm<sup>3</sup>. Neglecting minor changes in mineral density at pressure increase up to 100 MPa and using the formula (2), we obtain that the porosity of the sample *PL367* is equal to 1 % at 100 MPa. Given that the porosity of the sample at the atmospheric pressure is 1.6 %, we obtain the porosity estimation dependent on microcracks as 0.6 %.

The preferred orientation of cracks of given shape (ellipsoidal inclusions) was determined according to the distribution of the *D* value (see Fig. 5). Directions with the largest changes in  $V_P$  at the pressure increase, i.e. position of maximums at *D* distribution, correspond to the directions of normals to the microcrack planes. Therefore, the spatial orientation of microcracks in the sample *PL367* was described with  $\delta$ -function as in the case of DFO of monocrystal with the single rotation at 15° around the *Y* axis.

Elastic properties of the less porous sample *OKU2* at the pressure 0.1 MPa were simulated in the same way. The properties of the mineral matrix were described by experimental values of elastic moduli at 200 MPa. Since the confining pressure had no significant influence on the anisotropy and velocities of elastic waves in this sample (see Fig. 4), then the presence of pores and microcracks was modeled with the value of porosity at a pressure of 0.1 MPa. Preferred orientation of elongated pores was set, as in the case of the sample *PL367*, by  $\delta$ -function according to the *D* distribution (see Fig. 5).

Distributions of the phase velocities of *P*- and *S*-waves of the samples *OKU2* and *PL367* in regard of the observed theoretical models are shown in Fig. 9.

The presented contour maps of  $V_P$  for the models with different properties of mineral matrix correspond with experimental distributions obtained at the pressure of 0.1 MPa. However, the best correspondence with experimental data for *P*-waves is observed for the models with elastic moduli of mineral matrix restored at the pressure of 200 MPa for the sample *OKU2* (see Fig. 4, *a*) and 100 MPa for *PL367* (see Fig. 4, *b*). For *S*-waves, data of modeling with regard of cracks is in good correspondence with the results of ultrasonic measurements at the atmospheric pressure only in the sample *OKU2* (see Fig. 9), when the mineral matrix with elastic properties of the sample *OKU2* at the pressure of 200 MPa was used as a model.

For the sample *PL367*, results of theoretical modeling, based on experimentally obtained elastic moduli at the pressure of 100 MPa, describe the nature of distribution of the measured velocities of *S*-waves only qualitatively, because there is a matching only of maximum and minimum velocity values of  $V_{S1}$  and splitting  $dV_S$ .

## Discussion

The studied samples represent two typical cases of geological media with different structural features and degree of anisotropy of elastic properties. Comparison of the results of theoretical modeling with experimental values of the phase velocities  $V_P$  and splitting  $dV_S$  of *S*-waves velocities at different pressures showed significant differences, especially for the sample of layered gneiss *PL367*.

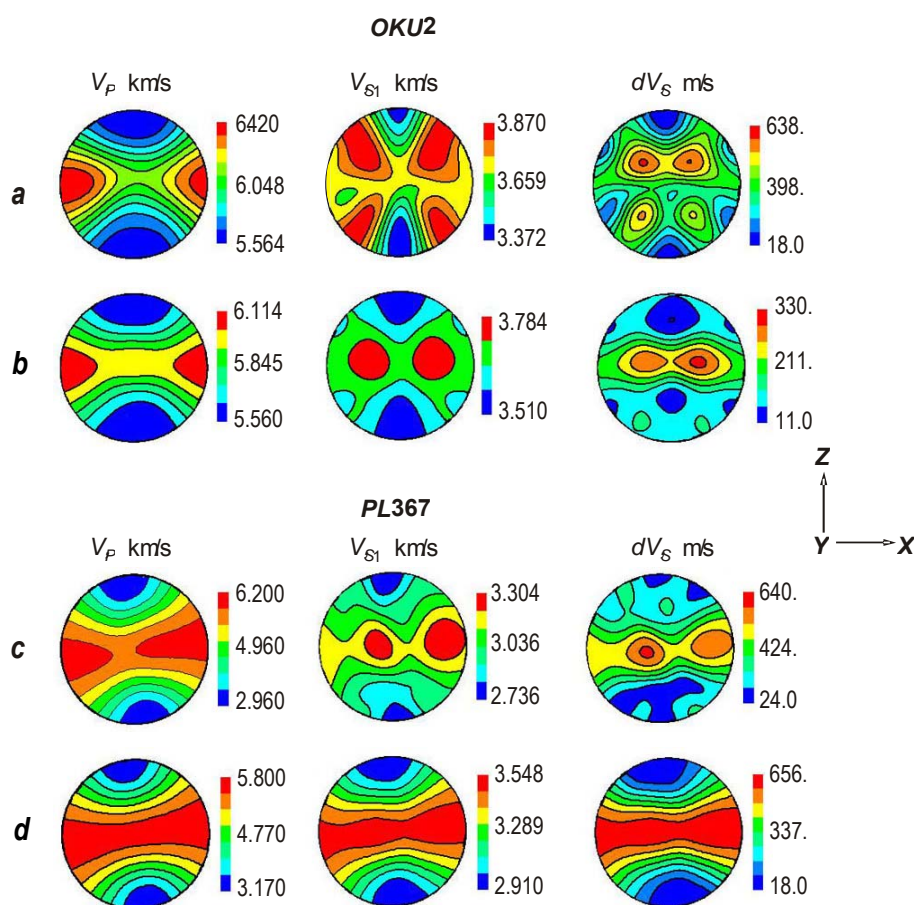


**Fig. 9.** Contour maps of phase velocities  $V_P$  (first column),  $V_{S1}$  (second), and splitting  $dV_S$  of the velocities of  $S$ -waves (third) theoretically calculated according to various mathematical models for the two studied samples.

Sample *OKU2*: modeling with the properties of the mineral matrix based on velocity measurements of  $P$  and  $S$ -waves at the pressure of (a) 200 MPa and (b) by the *GEOMEAN* model;

Sample *PL367*: modeling with the properties of the mineral matrix based on velocity measurements of  $P$  and  $S$ -waves (c) at the pressure 100 MPa and (d) by the *Backus* model

In heterogeneous media (striking example of such media is a layered medium), the propagation of elastic waves is accompanied by multiple dispersion at heterogeneities that causes the dispersion of velocities of elastic waves. If the length of elastic wave  $\lambda$  significantly exceeds the size of heterogeneities  $L$  (long-wave case), the velocities of elastic waves passing through the heterogeneous medium will not depend on the wave length. Thus, the measured velocity values describe the effective elastic properties of heterogeneous medium as if this medium was homogeneous. Therefore, the fulfillment of condition of the long-wave approximation

$$R = \frac{\lambda}{L} \gg 1 \quad (3)$$

is necessary for comparison of results of theoretical modeling with experimentally measured velocity values in the rocks.

For velocities of  $P$ - and  $S$ -waves in the sample *PL367* at pressures up to 100 MPa, the minimum value of  $R$  is about a unity that apparently caused disagreement in results of theoretical modeling (Figs. 8 and 9) and velocity values obtained experimentally (Fig. 4). From the comparison of Figs. 4, 8, and 9 it also obviously follows that velocities of shear

waves in the sample *PL367* proved to be more sensitive to its layered structure, especially at the atmospheric pressure. This is due to the presence of microcracks in the layers that significantly increase the contrast of elastic properties of the layers and consequently leads to the higher dispersion of elastic waves and thus to the dispersion of *S*-waves velocities.

The contrast of elastic properties of the minerals in the sample *PL367* also affects the elastic anisotropy of effective properties calculated according to different micromechanical models. In the anisotropic rock sample, the layering and shape texture contribute to the total elastic anisotropy depending on the crystallographic texture of minerals. The weak contrast of elastic properties of minerals, sharpness of crystallographic texture of biotite and muscovite were the reasons that different theoretical models in general slightly differ from each other for the sample *PL367*, and the main factor that controls the elastic anisotropy is the preferred orientation of grains of biotite and muscovite (Fig. 6).

Similar estimates of the contrast of elastic properties are also valid for a more homogeneous sample *OKU2*. However, the difference between experiment and theory in this case cannot be explained by a violation of the condition of the long-wave approximation. Most likely, the differences can be caused by the fact that the used theoretical methods of calculation of effective properties are based on the assumption of homogeneity of stresses and strains inside each phase of multiphase medium. Such approximation actually may not correspond to the distributions of the local stresses and strains in the minerals grains.

One of the features of this work is the use of nonlinear approximation (1) for the estimation of properties of the mineral matrix and the influence of microcracking. The distribution of coefficient *D* (Fig. 5) correlates well with the preferred orientation of micas obtained according to the data of neutron diffraction texture analysis. Apparently, in the micas of the studied samples, there is a system of oriented grain boundaries, cracks, and elongated pores associated with the crystallographic texture and properties of muscovite and biotite. This is confirmed by a good correspondence of the results of theoretical modeling of experimentally established distributions of *P*-wave velocities at 0.1 MPa for the sample *PL367* (Fig. 4, *b* and Fig. 9, *c*) and *P*- and *S*-wave velocities at 0.1 MPa for the sample *OKU2* (Fig. 4, *a* and Fig. 9, *a*).

It is also shown that elastic properties of the rocks containing cracks and pores significantly depend on the properties of textured mineral matrix. This affects the results of estimation of porosity and other parameters of void volume carried out on the basis of experimental data on elastic waves velocities (see, for example, [Bayuk, Ryzhkov, 2010]). The noted fact is important for practical problems in the study of oil- and gas-bearing rocks.

## Conclusions

Using the comprehensive approach that includes the neutron diffraction texture analysis, ultrasonic measurements of elastic wave velocities, and theoretical modeling, we carried out an investigation of elastic anisotropy of highly anisotropic sample of plagioclase-biotite gneiss and sample of biotite gneiss with weak anisotropy. For the first time the experimental spatial distributions of velocities of *P*- and *S*-waves were obtained for the samples of layered rocks.

The theoretical modeling of effective elastic properties of the sample was performed by different methods and showed that the main factor controlling the anisotropy of elastic properties of the studied gneiss samples is the preferred orientation of micas grains (muscovite and biotite). The display of heterogeneity in the structure (compositional layering) and also the presence of heterogeneous stresses and strains inside the crystallites affects the

experimentally measured velocities of  $P$ - and  $S$ -waves and, ultimately, lead to the observed differences between the results of ultrasonic measurements and theoretical modeling.

For the first time in this work the nonlinear approximation of dependence of  $P$ -wave velocities on the pressure was applied to estimate the elastic properties of the mineral matrix and preferred orientation of plane cracks and elongated pores in the sample volume. The correlation of coefficient  $D$  distribution was determined in the nonlinear approximation with crystallographic texture of mica that governs the orientation of grain boundaries and presence of oriented microcracks in the grains of these minerals.

On the example of studied samples it is shown the importance of determining the elastic properties of the mineral skeleton in solving problems of crack-porous space in rocks on the basis of seismic and acoustic methods and theoretical modeling.

### Acknowledgments

The work was partly supported by Authorized representative of the Czech Republic in the Joint Institute for Nuclear Research (JINR, order No. 189 of 29.03.2016, p. 27), the Cooperation program of JINR – the Czech Republic (order No. 155 of 14.03.2016, p. 26), as well as a contract MSMT Kontakt II – LH13102, projects of the Grant Agency of the Czech Republic 13-13967S, and the long-term research topic No. RVO67985831 of the Institute of Geology, Academy of Sciences of Czech Republic.

Experiments with the use of neutron dispersion were performed with the texture diffractometer SCAT at the research nuclear installation IBR-2 in the laboratory of neutron physics of the Joint Institute for Nuclear Research (Dubna, Russia).

### References

- Aleksandrov K.S. and Prodajvoda G.T., *Anizotropiya uprugih svojstv mineralov i gornyh porod* (Anisotropy of elastic properties of minerals and rocks), Novosibirsk: Publishing House SB RAS, 2000.
- Babuska V. and Cara M., *Seismic Anisotropy in the Earth*, Kluwer Academic Publishers, Dordrecht. 1991.
- Backus G.E., Long-wave elastic anisotropy reduced by horizontal layering, *J. Geophys. Res.*, 1962, vol. 67, pp.4427–4440.
- Bass J.D., Elasticity of minerals, glasses, and melts, in *Mineral Physics and Crystallography: A Handbook of Physical Constants*. AGU Ref. Shelf, vol. 2. Edited by T. J. Ahrens. AGU. Washington D. C. 1995.
- Bayuk I.O. and Ryzhkov V.I., Opredelenie parametrov treshchin i por karbonatnykh kollektorov po dannym volnovogo akusticheskogo karotazha. *Tekhnologii sejsmorazvedki*, 2010, no. 3, pp. 32–42.
- Birch F., The velocity of compressional wave velocities in rocks to 10 kbar, *J. Geophys. Res.*, 1961, vol. 66, pp.2199–2224.
- Crampin S., A review of wave motion in anisotropic and cracked elastic-media, *Wave motion*, 1981, vol. 3, pp.341–391.
- Ivankina T. I. and Matthies S., On the development of the quantitative texture analysis and its application in solving problems of the Earth sciences. *Physics of Particles and Nuclei*, 2015, vol. 46, no. 3, pp. 366–423.
- Keppler R., Ullemeyer K., Behrmann J.H., and Stipp M., Potential of full pattern fit methods for the texture analysis of geological materials: implications from texture measurements

- at the recently upgraded neutron time-of-flight diffractometer SKAT, *J. Appl. Crystallography*, 2014, vol. 47, pp.1520–1534.
- Kern H., P- and S-wave velocities in crustal and mantle rocks under the simultaneous action of high confining pressure and high temperature and the effect of the rock microstructure. In: Schreyer, W. (Ed.), *High-Pressure Researchers in Geoscience*. H. Schweizerhartsche Verlagsbuchhandlung, Stuttgart, 1982.
- Kern H., Ivankina T.I., Nikitin A.N., Lokajicek T., and Pros Z., The effect of oriented microcracks and crystallographic and shape preferred orientation on bulk elastic anisotropy of a foliated biotite gneiss from Outokumpu, *Tectonophysics*, 2008, vol. 457, pp.143–149.
- Kern H., Mengel K., Strauss K.W., Ivankina T.I., Nikitin A.N., and Kukkonen I.T., Elastic wave velocities, chemistry and modal mineralogy of crustal rocks sampled by the Outokumpu scientific drill hole: Evidence from lab measurements and modeling, *Physics of the Earth and Planetary Interiors*, 2009, vol. 175, pp.151–166.
- Kichanov S.E., Kozlenko D.P., Ivankina T.I., Rutkauskas A.V., and Savenko B.N., The neutron imaging and tomography studies of deep-seated rocks from the Kola superdeep borehole, *Physics Procedia*, 2015, vol. 69, pp.537–541.
- Lobanov K.V., Kazansky V.I., Kusnetsov A.V., Zharikov A.V., Nikitin A.N., Ivankina T.I., and Zamyatina N.V., Correlation of Archean rocks from the Kola superdeep borehole and their analogues from the surface: evidence from structural – petrological, petrophysical and neutron diffraction data, *Petrology*, 2002, vol. 10, no. 1, pp.23–38.
- Lokajicek T. and Svitek T., Laboratory measurement of elastic anisotropy on spherical rock samples by longitudinal and transverse sounding under confining pressure, *Ultrasonics*, 2015, vol. 56, pp. 294–302.
- Melia P.J. and Carlson R.L., An experimental test of P-wave anisotropy in stratified media, *Geophysics*, 1984, vol. 49, pp. 364–378.
- Schoenberg M. and Muir F., A calculus for finely layered anisotropic media, *Geophysics*, 1989, vol. 54, no. 5, pp.581–589.
- Shermergor T. D., *Teoriya uprugosti mikroneodnorodnyh sred* (The theory of elasticity of microinhomogeneous media), Nauka: Moscow, 1977.
- Vasin R.N., Wenk H.-R., Kanitpanyacharoen W., Matthies S., and Wirth R., Elastic anisotropy modeling of Kimmeridge shale, *J. Geophys. Res.: Solid Earth*, 2013, vol. 118, pp.1–26.
- Zel I.Yu., Ivankina T.I., Levin D.M., and Lokajicek T., Application of a modified method of ultrasonic measurements for determination of elastic moduli of rocks. *Crystallography Reports*, 2015, vol. 60, no. 4, pp. 537–545.
- Zel I.Yu., Ivankina T.I., Levin D.M., and Lokajicek T., P-wave ray velocities and the inverse acoustic problem for anisotropic media. *Crystallography Reports*, 2016, vol. 61, no. 4, pp. 623-629.